

Chapter 6

Advances in Fs-Laser Micromachining Towards the Development of Optofluidic Devices



João M. Maia, Vítor A. Amorim, D. Alexandre and P. V. S. Marques

Abstract In this chapter the developments made in femtosecond laser micromachining for applications in the fields of optofluidics and lab-on-a-chip devices are reviewed. This technology can be applied to a wide range of materials (glasses, crystals, polymers) and relies on a non-linear absorption process that leads to a permanent alteration of the material structure. This modification can induce, for instance, a smooth variation of the refractive index or generate etching selectivity, which can be used to form integrated optical circuits and microfluidic systems, respectively. Unlike conventional techniques, fs-laser micromachining offers a way to produce high-resolution three-dimensional components and integrate them in a monolithic approach. Recent advances made in two-photon polymerization have also enabled combination of polymeric structures with microfluidic channels, which can provide additional functionalities, such as fluid transport control. In particular, here it is emphasised the integration of microfluidic systems with optical layers and polymeric structures for the fabrication of miniaturized hybrid devices for chemical synthesis and biosensing.

J. M. Maia (✉) · V. A. Amorim · P. V. S. Marques

Department of Physics and Astronomy, Faculty of Sciences of University of Porto, Rua do Campo Alegre 687, Porto, Portugal
e-mail: joao.m.maia@inesctec.pt

V. A. Amorim
e-mail: vitor.a.amorim@inesctec.pt

P. V. S. Marques
e-mail: psmarque@fc.up.pt

D. Alexandre
Department of Physics, University of Trás-os-Montes e Alto Douro, Quinta de Prados, 5001-801 Vila Real, Portugal
e-mail: daniel@utad.pt

J. M. Maia · V. A. Amorim · D. Alexandre · P. V. S. Marques
CAP - Centre for Applied Photonics, INESC TEC, Rua Dr. Roberto Frias, Porto, Portugal

6.1 Introduction

Lab-on-a-chip systems correspond to miniaturized devices capable of performing several functions, which are typically realized in a full scale laboratory [1, 2]. These devices consist of a network of microfluidic channels (with a usual cross-section size of 10–100 μm) that are ended by reservoirs or inlet/outlet ports, which allow connection with tubes for fluid pumping. The small dimension of these microfluidic channels introduces unique properties in the kinematics of the fluid flow, which has strong implications in basic processes. In particular, these channels can be used for transport of fluids, for mixing of different reagents or for control of the concentration of particles present in the stream [3]. Microfluidic systems can also be combined with other components (electrical or optical) for active control of the flow or for sensing applications in medical and biochemical environments [4, 5]. Regarding the latter application, these systems can alleviate some issues related to long analysis time and high reagent consumption, while at the same time maintaining high accuracy and performance.

Photolithography and etching were the first technique used for the development of microfluidic devices on silicon and glass and are still one of the main technologies used in planar lightwave circuit technology [6, 7]. Despite its maturity, this technique presents some limitations: (a) it is a planar technique, meaning that the devices are made at the substrate's surface which limits the maximum density of components that can be integrated, and (b) it is a multistep technique that requires access to a specialized cleanroom facility. In particular, the high cost of this method has promoted the development of new microfabrication techniques (soft lithography, injection molding and hot embossing) which use polymers (PDMS—polydimethylsiloxane, PMMA—polymethylmethacrylate) as a target material and rely on replication of a mold [8, 9]. Despite allowing rapid prototyping of microfluidic structures with submicrometer resolution, these methods possess some issues: (a) like all methods based on photolithography they are planar, and (b) integration of microfluidics with optical layers is pretty challenging given that polymers typically exhibit higher propagation losses and poorer light confinement than glasses, not to speak on the difficulties of the fabrication methods.

In order to overcome these issues, fs-laser micromachining has been adopted for the production of lab-on-a-chip devices. In this technique, a sample (glass, crystal or polymer) is scanned by a focused laser beam which gives rise to a non-linear interaction between the laser beam and the irradiated material. This interaction leads to a permanent modification of the material confined within the focal volume, thus submicrometer resolutions can be obtained [10]. Depending on the pulse characteristics (wavelength, repetition rate, laser fluence) and on the material used different modifications can occur, namely variation of the refractive index (either positive or negative), generation of etching selectivity, formation of voids, among other effects. These modifications have led to the formation of different systems: optical circuits [11], electrical layers [12], microfluidic systems [13], polymeric structures [14] that can be fabricated either separately or integrated in a single chip. Additionally, the

inherent three-dimensional aspect of this technology accounts for a flexible system design and for high component integration.

The possibility of combining microfluidic systems with optical layers and polymeric structures in a monolithic glass block provides a unique opportunity for the design of optofluidic devices with far-reaching applications in basic science, chemical synthesis and drug development, and biochemical analysis [15, 16]. Thus, the goal of this chapter is to discuss recent advances made in fs-laser micromachining to fulfil the production of such devices. After this introduction, the fundamentals of fs-laser micromachining are discussed. The types of structural modifications that can be obtained are reviewed, alongside with the materials in which these modifications can be observed. Some examples of existent devices for applications in optical communications and in microfluidics are presented. Then, novel optofluidic devices for on-chip optical sensing and particle manipulation are reviewed. A summary of future developments expected for this field is also presented.

6.2 Femtosecond Laser Micromachining

In a typical laser direct writing setup, the fs-laser beam is focused inside a material transparent to the beam wavelength through a focusing lens, as shown in Fig. 6.1. The most common fs-laser systems used for micromachining are regeneratively amplified Ti:sapphire lasers (fundamental wavelength of 800 nm) and Ytterbium-based lasers (fundamental wavelength of 1030 nm); wavelengths other than the fundamental can be used by generation of second or third harmonic. Several free-space optics components can be used to, for example, control the beam polarisation (through a half-wave plate), or to adjust the beam spot size to the lens entrance diameter (through a beam expander). External components can also be used to control the pulse energy. The sample is positioned by three motorized stages and is scanned relative to the beam propagation direction across any spatial direction. In certain systems, beam scanning techniques that use galvanometric mirrors are combined with sample scanning for an improved exposure.

6.2.1 *Fundamentals of Interaction Laser-Matter*

The interaction between the laser beam and the material can generate many modifications, which are at the basis of the formation of several types of devices. Although the fundamentals of this interaction is still a topic under discussion and depends on the material used, a simple and common qualitative model is generally accepted. This model involves generation of a free electron plasma followed by energy relaxation and alteration of the material structure. Here, the basic principles of this interaction are presented; a more detailed analysis can be found elsewhere [10].

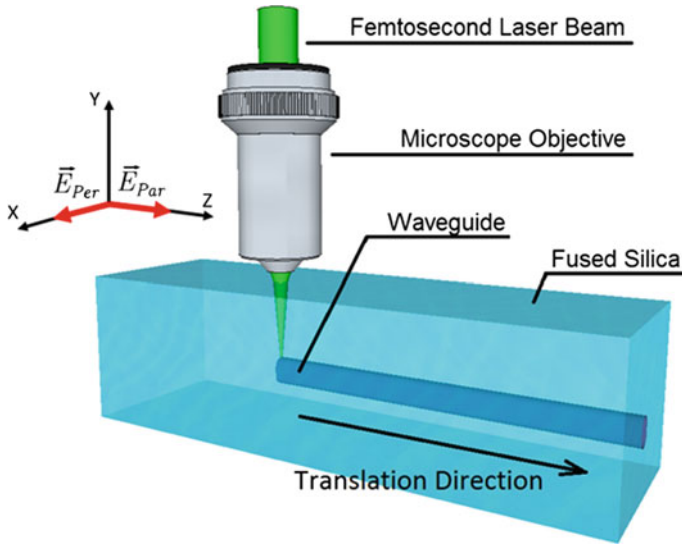


Fig. 6.1 Overview of the laser writing process: optical components are fabricated by writing a single track, while microfluidic channels are usually fabricated by stacking multiple tracks, as described in [17]

A fs-laser pulse, being focused inside a sample, does not have sufficient energy to be linearly absorbed due to the large band gap of the material. However, the high peak intensities of fs-laser pulses (around 10 TW/cm^2) can promote electron transition from the valence band to the conduction band via non-linear absorption. This process is started by multiphoton ionization and/or tunnelling ionization that seed avalanche ionization. Multiphoton ionization corresponds to absorption of multiple photons by an electron at the valence band. The net energy absorbed by the electron is bigger than the band gap energy, thus the electron can transit to the conduction band. Tunneling ionization corresponds to the deformation of the band gap structure due to the strong electric field, which lowers the band gap energy and enables direct transition from the valence band to the conduction band through quantum tunneling. These two processes can occur either simultaneously or separately, depending on the laser intensity and frequency, and their influence can be described by the Keldysh parameter. Both of these processes increase the density of electrons present in the conduction band and act as seed for avalanche ionization: electrons present in the conduction band can excite an electron in the valence band due to collisional ionization. These two electrons, at the conduction band, while exposed to the laser field can absorb laser energy and repeat this process, giving rise to an exponential growth in the number of electrons present in the conduction band. The free electrons form a highly absorbing plasma that oscillates at a frequency that increases with the density of free electrons. In a couple of picoseconds, the plasma frequency matches the laser frequency and the plasma transfers its energy to the lattice. Within the microsecond timescale, heat

diffuses away from the irradiated region which melts and resolidifies. If the energy deposited in the lattice is above a threshold level, the material structure is permanently modified. It is possible, however to distinguish between two cases, depending on the pulse repetition rate. At high repetition rates the time between consecutive pulses is shorter than the time for thermal diffusion and heat builds up around the focal volume, while at low repetition rates thermal equilibrium is obtained long before new irradiation. In either case, the modification is confined to the focal volume, and therefore submicrometer resolutions can be obtained.

Different modifications can be produced depending on the pulse characteristics (duration, repetition rate, energy, wavelength) and on the setup used (objective lens and numerical aperture, stages scanning speed, polarisation of the laser beam relative to the scanning direction). This text only focuses on the interactions that enable fabrication of optical circuits, microfluidic systems and polymeric structures. Other induced phenomena can be found elsewhere [10, 18].

6.2.2 *Fabrication of Optical Elements*

One of the possible modifications resulting from the laser-matter interaction is related to the variation of the refractive index around the focal volume, which can enable fabrication of either passive or active optical components. This modification can be observed in a wide range of materials, but here we focus our attention to fused silica, due to its importance in the optoelectronic industry and its properties, namely chemical and thermal stability and biocompatibility.

Considering the interaction between a fs-laser pulse and fused silica, at low pulse energies slightly above the modification threshold it is observed an increase of the refractive index. The index variation is generally attributed to two mechanisms, densification and formation of colour centres, whose contribution depends on the processing conditions. Densification results from the rapid melting and solidification of the material in the focal volume [19], and has been shown to be linearly related with the refractive index in fused silica [20]. Formation of colour centres, which are defects in the lattice periodicity lead to a change in the refractive index through the Kramers–Kronig mechanism [21]. Analysing the cross-section of the modification pattern, it corresponds to an elongated inverted droplet shape, where the top region is associated to a decrease of the refractive index, while the bottom region is associated with an increase of the refractive index, Fig. 6.2a. By translating the sample in relation to the beam focus, as shown in Fig. 6.1, it is then possible to produce type I optical waveguides embedded in the silica slab, where light is confined to the bottom region. The quality of the waveguides, namely insertion losses and mode field diameter, strongly depends on the irradiation conditions (orientation of the beam polarisation relative to the scanning direction, writing depth, scanning speed, pulse energy) and on the laser pulse characteristics, thus each laboratory may obtain low-loss waveguides at different processing parameters. Of significant interest is the production of single-mode low-loss waveguides at the telecommunication

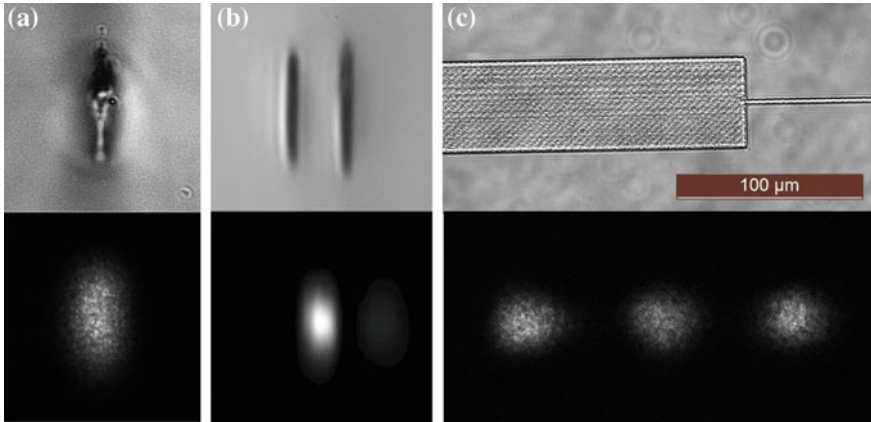


Fig. 6.2 Optical microscope image of the cross-section and mode profile **a** at 1550 nm of type I waveguides made in fused silica and **b** at 633 nm and TM polarization for type II waveguides made as a double line structure with 10 μm separation in x -cut LiNbO_3 . **c** 1×3 MMI splitter made in fused silica, with a top view image of the device shown on top (light is incident from the right) and the intensity distribution at 1550 nm shown at the bottom. Image (**b**) was reproduced from [42] (Applied Physics A: Materials Science and Processing, Origins of waveguiding in femtosecond-laser structured LiNbO_3 , volume 89, 2017, page 132, J. Burghoff, S. Nolte, and A. Tünnermann), © Springer-Verlag 2007, with permission of Springer

wavelength for optical communication devices. By optimizing the irradiation conditions, Fukuda et al. fabricated single-mode waveguides with minimum propagation losses of 0.05 dB/cm in fused silica [22]. The index variation is around 10^{-3} and the mode field diameter of the waveguide matches the mode field diameter of a standard single-mode fiber ($\sim 10 \mu\text{m}$). Nevertheless, the waveguide mode is asymmetric, and in order to correct this issue several beam shaping techniques have been proposed which consist of slit focusing, astigmatic focusing or multiscan writing [23, 24].

Besides fused silica, other glasses have also shown an increase of the refractive index when exposed to a fs-laser beam. Eaton et al. [25] have fabricated single-mode waveguides in borosilicate glass with propagation losses of 0.2 dB/cm at 1550 nm. They verified that by writing in the high repetition rate regime, the accumulated heat would favour a uniform index distribution and enable production of waveguides with circular cross-section. Ams et al. [26] also wrote waveguides in phosphate glass, having obtained a minimum loss of 0.39 dB/cm at 1550 nm. In this case, a slit was placed in front of the focusing lens in order to shape the beam profile, and obtain symmetric waveguides.

Due to the index modification, several passive elements have already been demonstrated. By making use of the three-dimensional motorized stages, several groups have reported S-bended waveguides with minimum bend losses [22, 27]. This concept was further developed by Thomson et al. [24] where a fan-out device was fabricated in a silica glass chip to couple light from a fiber V-groove array to a multicore optical fiber. Modulation of the fs-laser beam pulse spectrum has also been applied

to the production of grating waveguides. By adjusting the stages scanning speed and modulation frequency, first-order Bragg gratings can be produced with tunable Bragg wavelength. Ams et al. [28], for instance, have fabricated Bragg gratings in a silicate glass with a high coupling coefficient of 1457 m^{-1} , enabling much shorter device lengths. Grenier et al. [29] and Zeil et al. [30] also developed new writing techniques to tailor the grating's coupling strength, which enabled the production of phase-shift and apodized gratings, respectively. Control of the waveguide birefringence for the design of beam splitters and wave retarders has also been demonstrated, by writing stress-tracks next to the optical waveguide [31].

Several optical devices for power splitting have also been reported in a wide range of configurations. Sohn et al. [32] and Liu et al. [33] have extensively studied fabrication of Y-junctions for 1-to-N power division with balanced splitting at 1550 nm. Recently, Amorim et al. [34] proposed a novel writing technique at the junction divergence point, in order to obtain uniform splitting in a broad spectral range (1300 nm to 1600 nm). Fabrication of directional couplers with several coupling ratios has also been reported by a correct adjustment of the interaction length and arm separation [35, 36]. Although, the work developed so far only served as proof-of-concept, multimode interference (MMI) devices for 1-to-N splitting have also been reported in two different configurations, where the multimode region is fabricated by stacking multiple scans close to each other, as shown in Fig. 6.2c [37, 38]. More complex designs, such as channel add-drop filters and arrayed-wave gratings, for channel multiplexing applications have also been reported [39, 40].

Plenty of attention has also been devoted to other materials (rare earth-doped glasses, chalcogenide glasses) and to the production of active elements, namely on-chip laser sources. The induced index variation provides a way to guide light through an optical waveguide, while the medium properties contribute to light amplification. Besides the type I waveguides previously described, two other configurations can be used. In type II waveguides (Fig. 6.2b), an unexposed region surrounded by two damaged regions acts as core: the two damaged regions alter the stress field around the irradiated volume, leading to an index variation through the strain (or stress)-optic effect [41, 42]. The laser-matter interaction can also produce a negative index region, from which depressed cladding waveguides can be obtained where the core is surrounded by irradiated tracks of lower index [43, 44]. These geometries are generally preferred in active waveguides, because the core is not irradiated and, therefore, the medium properties are left unchanged.

Many near infrared continuous-wave laser sources have already been reported in Yb, Nd, Er, Pr doped crystals and glasses [45, 46]. Zhang et al. [47] demonstrated laser oscillation at 1061 nm with a slope efficiency of 25% and maximum output power of 11 mW by fabricating type II waveguides in a Nd:GGG crystal. Palmer et al. [48] reported a depressed cladding waveguide with high index contrast (2.3×10^{-2}) made in Yb-doped glass and demonstrated laser oscillation at 1030 nm in Yb:ZBLAN glass with a slope efficiency of 84% and maximum output power of 170 mW. Della Valle et al. [49] also developed a single longitudinal mode laser emitting at 1550 nm with a slope efficiency of 21% and maximum output power of 50 mW, consisting of a type I waveguide made in Er–Yb-doped phosphate glass. Operation

of these devices is based on direct light pumping from a standard optical fiber to a laser written optical waveguide. The cavity feedback elements can be produced by deposition of a reflective coating layer or by integration with external fiber Bragg gratings. The development of a robust monolithic cavity can be achieved by fs-laser writing of Bragg grating waveguides in the sample.

Production of waveguides in chalcogenide glasses has also been explored, with McMillen et al. [50] having reported minimum propagation losses of 0.65 dB/cm in gallium–lanthanum–sulfide chalcogenide glass. The properties of this medium make it highly attractive for the production of nonlinear components, besides laser sources. Hughes et al. [51] have demonstrated spectral broadening of a pulse with duration of 200 fs and wavelength of 1540 nm from an initial width of 50 nm to a final width of 200 nm, in gallium–lanthanum–sulphide glass. Psaila et al. [52] also demonstrated supercontinuum generation in a waveguide written in chalcogenide glass, where the pulse bandwidth increased from 100 to 600 nm.

Type I and type II waveguides can also be fabricated in lithium niobate, where the high electro-optic coefficient makes this glass suitable for the production of on-chip electric modulators [42, 53, 54].

6.2.3 *Fabrication of Microfluidic Systems*

The interaction between the fs-laser beam and matter can also enable fabrication of microfluidic devices. Production of these structures can be obtained in two different ways depending on the type of interaction (generation of etching selectivity or laser ablation).

Relatively to the former approach, glasses, when immersed in a hydrofluoric acid (HF) solution, are etched isotropically, meaning that all regions are etched at a similar rate. However, if the sample is first subjected to laser writing, then the irradiated regions will be more prone to the etching reaction than the remaining material. In fused silica, when the sample is exposed to a fs-laser beam, besides the refractive index variation, sub-wavelength birefringent structures, called nanogratings, can also be formed. These structures are responsible for the etching selectivity and consist of periodic layers of alternating refractive index, with a period around 100 nm. Formation of the nanogratings is based on the nanoplasmonic model proposed by Taylor et al. [55]. Thus, fabrication of microfluidic channels in fused silica is as follows: (i) the channel pattern is designed following the multiscan writing method (writing of multiple tracks with a separation of a couple of micrometers), (ii) the sample is then, usually, immersed in an HF solution [56]. The presence of the nanogratings leads to an anisotropic etching reaction, where hollow channels are formed inside the silica slab. This fabrication technique is commonly called fs-laser irradiation followed by chemical etching (FLICE).

Microfluidic channels can also be produced in Foturan glass. However, while in fused silica the generation of etching selectivity is based in a photophysical reaction, in Foturan glass it is due to a photochemical one [57, 58]. This photosensitive and

amorphous glass is composed by a lithium aluminosilicate matrix doped with trace amounts of a silver and cerium ions. When the laser beam is focused inside the glass, free electrons are generated by inter-band excitation, which reduces the silver ions to silver atoms. By performing a subsequent annealing process, at 500–600 °C, the silver atoms diffuse and agglomerate forming silver nanoclusters. The nanoclusters act as a seed for the formation of a crystalline lithium metasilicate phase that is etched in HF faster than the remaining amorphous material.

Although with limited success, generation of etching selectivity has also been reported in other materials. Matsuo et al. [59] have fabricated a square channel inside a quartz substrate, where selective etching was due to lattice amorphization. The issue was that the etch rate was of 50 $\mu\text{m/h}$, which resulted in a very long fabrication time. Formation of nanogratings was also verified in sapphire [60], which revealed an enhanced selectivity relatively to fused silica (100:1). The main limitations were the prolonged etching reaction which took several days and the accumulation of unetched material that recrystallized inside the channel. Choudhury et al. [61] also demonstrated that Nd:YAG crystals were selectively etched in an aqueous solution of H_3PO_4 , due to the creation of lattice defects and a certain degree of disorder. Though the etching reaction develops slowly, these results can pave the way for production of novel optofluidic devices with integrated laser sources.

The processing conditions affect the properties of the microfluidic channels (shape, surface roughness, aspect ratio) and the fabrication time (etch rate) [62–65]. Considering the formation of channels in fused silica, the orientation of the laser beam polarisation relative to the scanning direction influences the nanograting orientation and, consequently, the etch rate. If the polarisation is set orthogonal to the scanning direction, the etch rate is maximum because the nanogratings align with the channel axis (Fig. 6.3b). Meanwhile, for parallel alignment the HF finds alternate hollow and pristine layers that reduce the cumulative etch rate (Fig. 6.3a). The pulse energy can also affect the channel quality, given that higher pulse energies result in an increase of the stress field around the laser affected zones which can lead to channel deformation and appearance of microcracks [66]. The separation between modification tracks also influences the surface roughness, with lower separations giving rise to stress accumulation and consequent surface deformation, while higher separations result in accumulation of debris inside the channel. Production of channels with very low surface roughness is also possible by performing annealing after the etching reaction [67].

One of the issues inherent to the etching reaction is that the etch rate tends to saturate which leads to the formation of tapered channels with poor aspect ratio. This problem can be corrected by (i) suitably designing the channel so that it can compensate the tapering effect [68]; (ii) fabrication of openings connecting the channel to the glass surface which results in more access points for the acid to diffuse [17] (Fig. 6.3c); (iii) using potassium hydroxide instead of HF which eliminates the saturation effect at the expense of a lower etch rate [69].

In the FLICE method, channels with circular or rectangular cross-section (Fig. 6.3d) can be obtained by carefully patterning the modification tracks geometry [17]. Rectangular cross-sections are preferred for integration with optical waveg-

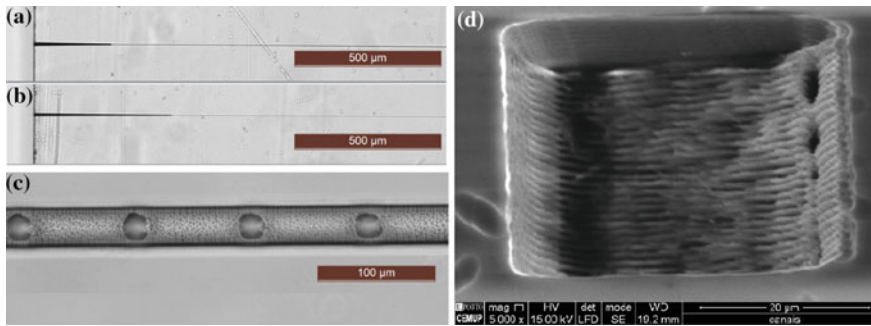


Fig. 6.3 Top view microscope images of microfluidic channels fabricated in fused silica with **a** parallel polarisation and **b** perpendicular polarisation; the remaining processing conditions and the etching time was the same in both cases. The darker regions correspond to hollow channels and, as can be seen, the etched length is bigger in **(b)** than in **(a)**, due to the beam polarisation orientation. **c** Top view image of a microfluidic channel made inside fused silica, which shows the access holes, connecting the channel to the silica surface, for acid diffusion. **d** SEM (Scanning Electron Microscope) cross-section image of a rectangular channel made in fused silica by FLICE

uides for cell trapping and stretching applications, while circular channels are better suited for developing on-chip biomimetic applications [46].

Another advantage of FLICE is that the microfluidic channels can be fabricated inside the glass, with the HF acid flowing through reservoirs that are made at the surface. This way it is not necessary to seal the final device and the reservoirs offer a simple way to connect tubes for fluid pumping [70]. Using this approach, Masuda et al. [71] have fabricated a Y-branched microfluidic channel for mixing of two fluids. One of the problems of this configuration is that the fluids only interact at the interface, which leads to an often slow and inefficient mixing process. To solve this issue, Liu et al. [72] developed a helical microchannel in fused silica that promoted a faster mixing reaction, by turning the usual laminar flow into a turbulent one. Due to the selective etching reaction, Sugioka et al. [52] also produced a pressure-actuated microplate inside the microfluidic channel that was used to switch the flow direction of reagents.

Laser ablation can also be used for production of microfluidic devices. At sufficiently high pulse energies, the laser-matter interaction can result in micro-explosions and formation of voids around the irradiated volume, which can be used as microfluidic channels [73]. Although this technique does not involve generation of etching selectivity and can be applied to a wider range of materials, some problems still stand. First, compared to FLICE the channel surface is typically rougher. Second, the channel length is limited to around 100 μm due to formation of debris that deposits along the channel. These issues can be minimized by performing the laser irradiation with the sample immersed in water, which flows through the channel removing the debris and smoothes the surface [74].

6.2.4 Fabrication of Polymeric Structures

Fs-laser micromachining can also be used in liquid resins or solid photoresists (that contain photoinitiators) to assist in two-photon polymerization. After fabricating the microfluidic channel, the channel is filled with the polymer and the fs-laser beam is scanned across it. The irradiation process leads to a two-photon absorption process, where two photons induce an electron transition from the ground state to an excited state. The excited electron then decays to the fundamental state emitting light in the ultraviolet to visible range. The photoinitiators present in the polymer absorb the fluorescent light and generate free radicals. The free radicals react with monomers, producing monomer radicals which react again with other radicals, thereby forming a polymeric chain. A detailed description of this process can be found in [75].

The polymerization reaction only occurs around the irradiated volume, while the unexposed zones can be rinsed in an appropriate solvent. This way, by scanning the laser beam across a determined pattern, 3D polymeric structures can be fabricated inside the microfluidic channel. The spatial resolution is around 100–200 nm, well beneath the diffraction limit and high aspect ratio structures can be fabricated. Additionally, the structures can be fabricated on top of any material, as long as the polymer can adhere strongly to it.

This technique has already been successfully applied to the fabrication of hybrid devices, which combine microfluidic channels and polymeric structures, for fluid mixing or particle filtering. Wang et al. [76] developed several filters consisting of a porous sheet, with variable shape and size (Fig. 6.4a). Therefore, only particles with a size smaller than the opening dimension could pass through the channel. Amato et al. [77] expanded on this concept and fabricated a filter to separate 3 μm polystyrene spheres in a Rhodamine 6G solution. Additionally, in a separate experiment they demonstrated filtering of red blood cells. However, after some time the particles would start to clog the channel.

Regarding mixers, Lim et al. [78], fabricated a polymeric structure after a Y-branched channel for mixing of two separate fluids (Fig. 6.4b). The structure con-

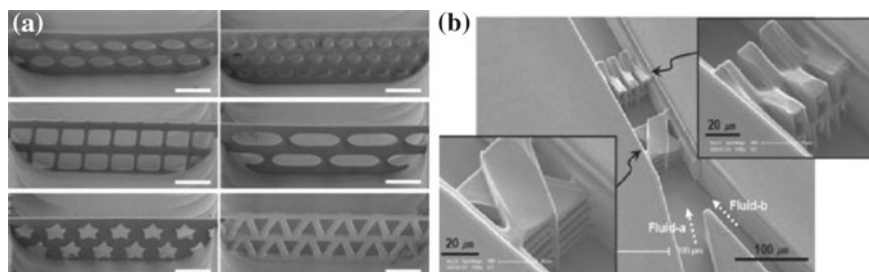


Fig. 6.4 SEM images of **a** microsieves with different openings sizes and shapes for particle filtering and **b** a crossing manifold micromixer embedded in a Y-branched channel. Images **(a)** and **(b)** were reproduced from [76, 78], respectively, with permission of ©The Royal Society of Chemistry

sisted of multiple layers, stacked vertically, which crossed each other in order to turn the flow chaotic. With this geometry, they predicted a mixing efficiency of 90%. Wu et al. [79] developed a similar device that could simultaneously filter and enhance mixing of different solutions, and thus significantly reduce the channel length. The structure consists of a mixer, with an equal configuration as in [78], which is placed in the middle of two sheets with periodic openings of constant dimension, which serves as filter. A mixing efficiency of 87% was obtained.

6.3 Integrated Optofluidic Devices

Fs-laser micromachining offers a unique way to integrate optical layers with microfluidic channels for cell manipulation and flow control applications or for on-chip optical sensing. Applegate et al. [80] were one of the first groups to show this integration for cell trapping and sorting. They fabricated a hybrid device where a microfluidic channel made by soft lithography in a PDMS slab was sealed against a fused silica substrate where optical waveguides were inscribed by fs-laser writing. The channel corresponds to a 1×4 splitter, and the system was assembled in such a way that the waveguides were set orthogonally to the channel and crossed it at the junction. Device operation relied on two laser beams: one beam was focused in the channel to excite the cell's fluorescence, and the other beam ($\lambda = 980$ nm) was coupled to the optical waveguide and was used to trap cells flowing through the stream (Fig. 6.5a). The latter beam was also used to manipulate the cell's position and direct it to a specific output branch, depending on the measured fluorescence. The fluorescence radiation was collected by a focusing lens and was detected by a CCD (charge coupled device) camera. This device was employed to successfully separate dyed-polystyrene particles with a diameter of $10 \mu\text{m}$ from non-fluorescent particles (Fig. 6.5b).

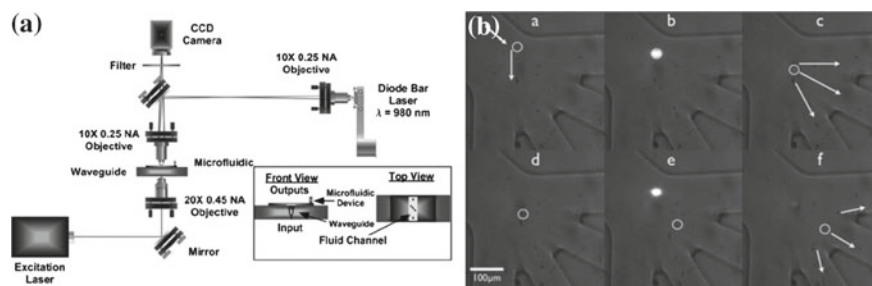


Fig. 6.5 **a** Schematic of an integrated microfluidic sorting system based on fluorescence detection. **b** Top view microscope image of a fluorescing particle being separated from a mixture of fluorescing and non-fluorescing particles. Reproduced from [80] with permission of ©The Royal Society of Chemistry

Using a similar principle, Hwang et al. [81, 82] developed an optofluidic device for cell detection and counting. The device was made in a fused silica chip entirely by fs-laser micromachining. The circular cross-section channel, made following the FLICE technique, exhibited a variable diameter that decreased from 100 μm at the entrance to 1–2 μm at the channel middle, which was smaller than the diameter of the particles used. This way, the particles would self-align and single cell detection was possible. An optical waveguide was inscribed perpendicular to the channel and crossing it at the smaller-sized segment. To detect particles, two distinct configurations were used as demonstrated in Fig. 6.6a, b. The first relied on measurement of the waveguide transmitted power, where the output power would vary whenever a particle crossed the waveguide. The second approach relied on detection of the cell fluorescence, which was induced by light propagating through the waveguide. In both cases, the number of peaks present in the fluorescence/intensity spectrum corresponds to the number of cells that crossed the waveguide (Fig. 6.6c). In particular, it was possible to detect red blood cells up to a flow rate of 0.5 $\mu\text{L}/\text{min}$.

Optical tweezers were also used to study the deformability properties of cells, given that the exerted optical force on the particle can cause it to stretch. In [15, 83] an optofluidic device was fabricated in fused silica, where optical waveguides

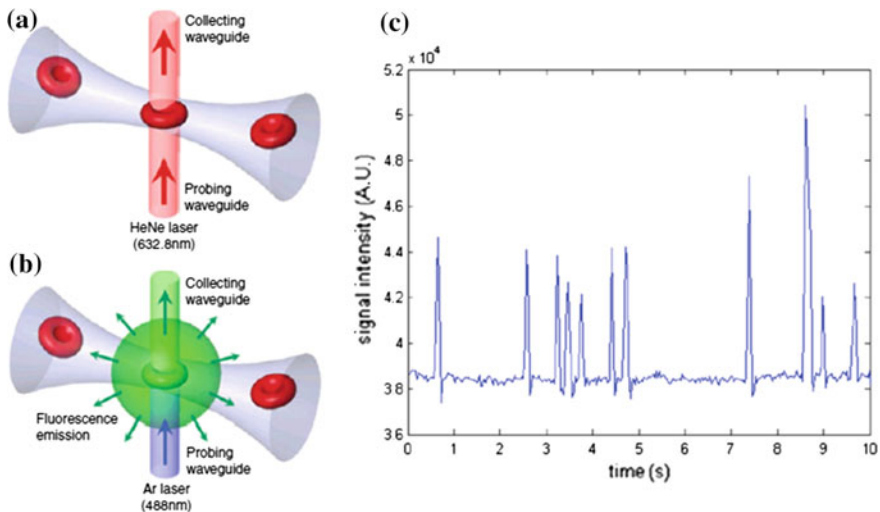


Fig. 6.6 Schematic of the integrated cell detection configuration: **a** measurement of transmitted power and **b** measurement of fluorescence radiation. **c** Output intensity spectrum as a function of time in a red blood cell counting experiment. The peaks present in the spectrum correspond to the passage of a cell through the waveguide. Images (a) and (b) were reproduced from [82] with permission of ©The Royal Society of Chemistry. Image (c) was reproduced from [81] (Applied Physics A: Materials Science and Processing, Three-dimensional opto-fluidic devices fabricated by ultrashort laser pulses for high throughput single cell detection and processing, volume 96, 2009, page 389, D.J. Hwang, M. Kim, K. Hiromatsu, H. Jeon, and C.P. Grigoropoulos), © The Author(s) 2009, with permission of Springer

were inscribed perpendicular to a microfluidic channel as described previously. A schematic of the proposed device is shown in Fig. 6.7. Light coupled to both waveguides was used to trap red blood cells that were flowing in a diluted blood solution. By adjusting the optical power in both waveguides, the cell position in the stream could be manipulated. In addition, by increasing the optical power it was observed that the cell would start to stretch along the optical trap axis. Due to the fused silica transparency, cell deformation could be observed in real time and its size could be easily measured. Study of these properties can be important in biomedical applications, given that the cell's deformability is related to its health. However, this approach is still limited given that the channel curvature and surface roughness cause deformation of the cell contour, which limits measurement resolution.

Using laser-induced fluorescence and optical stretching, other cell sorting configurations were also reported. Bragheri et al. [84] developed an optofluidic device formed by an X-shaped channel, where a single straight channel bifurcates at both ends into two 45° angled branches. The straight waveguide is interrogated by two optical waveguides (fluorescence waveguide and sorting waveguide), as shown in Fig. 6.8. The device was made in fused silica by fs-laser micromachining. In this system, a liquid containing the cells is injected in one inlet and a buffer solution is injected in the other outlet. Both solutions mix in the straight channel segment and, by adjusting the flow rate, all cells can leave through one of the outlets (OUT1). Light propagating through the fluorescence waveguide is focused in the microfluidic channel and is used to excite the cells' fluorescence. Radiation emitted by the cell is detected by a CCD camera placed on top of the channel; if the cell is fluorescent then the sorting waveguide is used to trap the cell and direct it into the other outlet

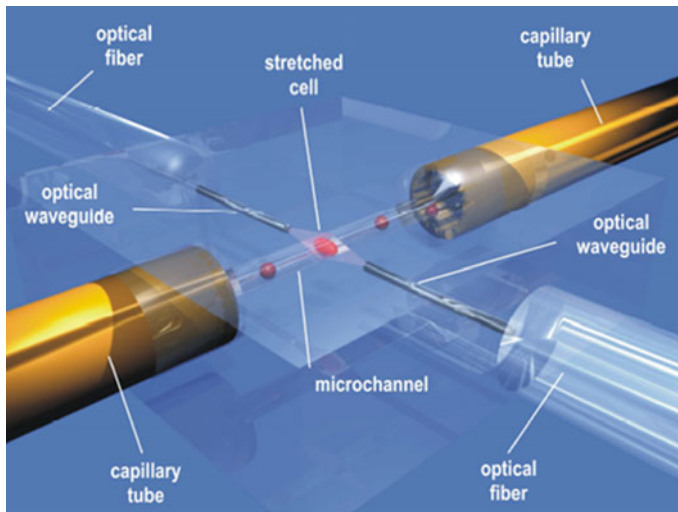


Fig. 6.7 Schematic of the monolithic optical stretcher for study of cell's deformability properties. Reproduced from [15] with permission of The Optical Society (© 2010 OSA)

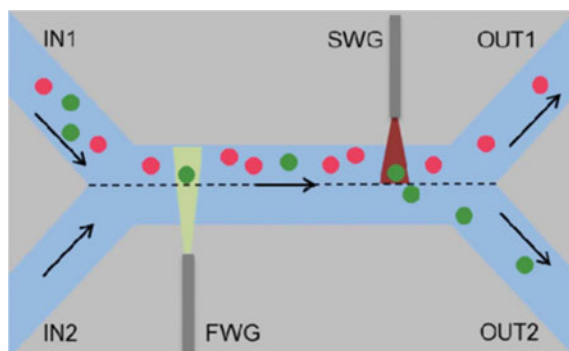


Fig. 6.8 Schematic of the device for cell sorting based on particle fluorescence (green and red particles correspond to fluorescent and non-fluorescent particles, respectively; FWG and SWG correspond to the fluorescence and sorting waveguide, respectively). Reproduced from [84] with permission of ©The Royal Society of Chemistry

branch (OUT2). This device was successfully used to sort, in real time, fluorescent polystyrene beads with a diameter of 7 μm . Yang et al. [85] used a similar device to sort melanoma cells based on their deformability. In this case, light propagating through the waveguide was used to first trap the cell, then to induce cell stretching by increasing the optical power, and finally to direct the cell to a specific branch. Cell deformation was evaluated in real time by imaging the cell and analyzing its shape as a function of the optical force exerted on it.

In microfluidic channels, electrokinetics is one of the main driving mechanisms of fluid flow due to the low surface-to-volume ratio of these systems. Therefore, capillary electrophoresis (separation of particles based on their electrical mobility) is highly attractive in microfluidic devices for the analysis of biomolecules in clinical applications. Chips for capillary electrophoresis are already commercially available and typically consist of two channels (one for injection and one for separation) crossing at 90° (Fig. 6.9). Each channel is terminated by two reservoirs with deposited electrodes, for application of a voltage difference across the channel. Operation of these chips is as follows: (i) a fluid is drawn into the injection channel and fills it due to electrokinetic flow, by applying a voltage difference across the channel; (ii) the injection channel is then kept at the same potential, while an electric field is applied across the separation channel; (iii) the fluid starts to flow along the separation channel and different species present in the stream flow at different speeds, due to the different electrophoretic mobility. By placing a detector at the separation channel end, the different species can be identified based on their arrival times. Vazquez et al. [86] used laser-induced fluorescence for particle detection. They used a commercial capillary electrophoresis chip (model D8-LIF from LioniX BV) and wrote an optical waveguide perpendicular to the separation channel, as shown in Fig. 6.9. Light at 532 nm was coupled to the waveguide via an optical fiber to excite fluorescence and an optical fiber, placed on top of the channel, was used to

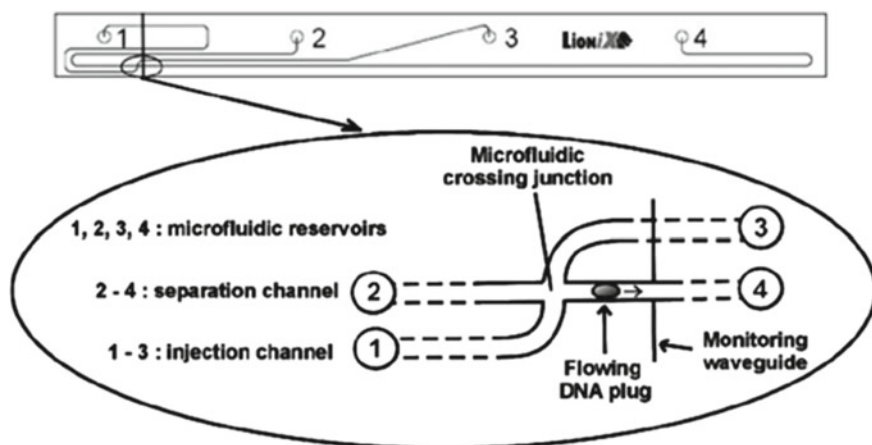


Fig. 6.9 Schematic of a capillary electrophoresis chip with an optical waveguide at the end of the separation channel for particle detection. Reproduced from [87] with permission of The Optical Society (© 2008 Optical Society of America)

collect the emitted radiation. The device was tested by using a solution of Rhodamine 6G (R6G) dissolved in a phosphate buffer. By increasing the R6G concentration, the intensity of the fluorescent signal detected increased linearly. In particular, low analyte concentrations of 40 pM were detected. Dongre et al. [87] used a similar configuration, but injected different rhodamine solutions (R6G and rhodamine-B) simultaneously in the channel. In the end, they were able to distinguish the different species by observing two different peaks in the fluorescent intensity spectrum, which corresponds to two different arrival times. In a separate experiment, Dongre et al. [88] fabricated a capillary electrophoresis chip in a fused silica slab by photolithography and etching and, after obtaining the chip, inscribed an optical waveguide by fs-laser writing as described previously. In order to maximize the detection resolution: (i) the channel walls were coated with a polymer to suppress electro-osmotic flow and minimize particle adsorption to the channel wall, and (ii) the channels were filled with a sieving gel matrix to induce a size-dependent variation in particles that exhibit a very similar mobility. In this case, they were able to detect double-stranded DNA molecules (labelled with a fluorescent dye) with different sizes in the channel, by observing that the molecules arrived at the detection point at different times.

Fluorescence detection is a very sensitive detection technique that allows measurement of very low analyte concentrations. However, the species must be labelled with a fluorescent molecule which may affect the particle properties and interfere with some chemical reactions. Therefore, label-free detection configurations may be more desirable in certain applications. Maselli et al. [89] fabricated an optofluidic device in a fused silica chip for refractive index sensing, where a Bragg grating waveguide (BGW) was written in between two microfluidic channels. Both structures were written in the same laser writing process and, when immersing the chip

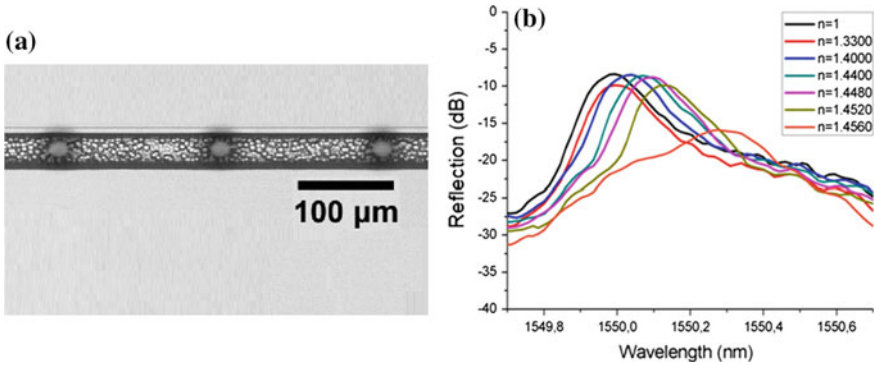


Fig. 6.10 a Top view image of a Bragg grating waveguide fabricated 3.8 μm from the microfluidic channel wall. The grating reflection spectrum obtained for this device is displayed in (b) for different fluid refractive indexes inside the microfluidic channel

in an HF bath, only the channel was etched while the waveguide remained unaffected. The separation between the BGW and each channel wall was 2 μm . The low separation between both structures enables evanescent interaction; thus light from a broadband source coupled to the waveguide is reflected at the Bragg wavelength. The reflected wavelength depends on the index of the fluid circulating in the channel (Fig. 6.10b). By filling the channel with solutions with different refractive index, a maximum sensitivity of 81 nm/RIU (refractive index unit) was obtained at the index 1.458, which represents a limit of detection of 1.2×10^{-4} . Additionally, compensation for temperature variation was achieved by fabricating a grating, with a different Bragg wavelength, outside the channel range. To obtain higher sensitivities, several solutions have been proposed: fabrication of phase-shifted gratings to engineer spectral defects or fabrication of a channel surrounding the entire channel. Recently, Maia et al. [90] monitored the etching reaction in situ, in order to precisely control the separation between the grating and the channel, which can also increase device sensitivity.

Higher sensitivities can be obtained in sensing schemes where there is a direct interaction between light and analyte. Hanada et al. [91] developed a sensor for detection of low chemical concentration based on absorbance measurements. The device was made in Foturan glass and the fabrication procedure encompasses the following steps: (i) the channel was inscribed by fs-laser writing followed by annealing and chemical etching in HF; (ii) a post-annealing process was realized to smooth the channel surface; (iii) the channel walls were coated with a polymer that had a lower index than water, in order to have light being guided along the channel; (iv) an optical waveguide was fs-laser written between the channel edge and the edge of the chip. The polymer coating process was essential to obtain a longer interaction length. The transmission spectrum was measured in a spectrometer: white light from a halogen lamp was coupled to the waveguide and transmitted through the microfluidic channel; the channel end was slightly tilted to direct light to the spectrometer,

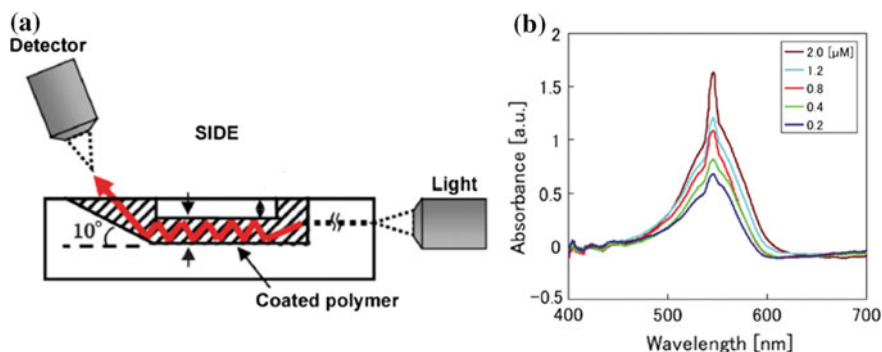


Fig. 6.11 a Schematic of the optofluidic chip for liquid concentration detection based on absorbance measurements. Figure b displays the corresponding absorbance spectra of glucose-D solutions with different concentrations. Reproduced from [91] with permission of ©The Royal Society of Chemistry

as depicted in Fig. 6.11a. The absorbance spectrum was obtained by subtracting the transmission spectrum of the liquid sample from the spectrum obtained for a hollow channel. The sensor was used, in two separate experiments, to detect trace amounts of protein (bovine serum albumin) and glucose-D. The measurements revealed that an increase of the species concentration resulted in a stronger absorbance (Fig. 6.11b); in particular a limit of detection of 7.5 mM and 200 nM was obtained for the protein and glucose-D, respectively.

Crespi et al. [16] also reported on a Mach–Zehnder interferometer integrated with a microfluidic system for refractive index detection. The entire device was made in a fused silica chip by fs-laser micromachining and a schematic is shown in Fig. 6.12a. In this device, light, from a broadband source, is coupled from an optical fiber to the optical waveguide and is splitted when it reaches the first Y-junction (because the interferometer is unbalanced, power splitting is not uniform). Then, one of the sensing arms of the interferometer crosses the channel (orthogonally to it), while the reference arm passes over the channel. The two arms then join in a second Y-junction, which leads to light interference. The output spectrum corresponds to periodically-spaced fringes. By changing the index of the fluid inside the channel, it is observed a shift in the fringe position which allows refractive index detection (Fig. 6.12b). The index detection can be related to other properties of the fluid. In this case, the channel was filled with different concentrations of aqueous glucose-D solutions, and a linear sensitivity of 1500 nm/RIU was obtained along the entire concentration range, which corresponds to a limit of detection of 1.5×10^{-4} RIU. In a separate experiment, peptide molecules, used in the pharmaceutical industry, were also detected with a limit of detection of 9 mM.

Microresonators can also be fabricated for generation of whispering gallery modes, in which specific resonances are confined to the cavity. These structures have unique properties, suitable for chemical and biosensing applications, such as high cavity quality factor and small resonator size. Lin et al. [92] used the selective

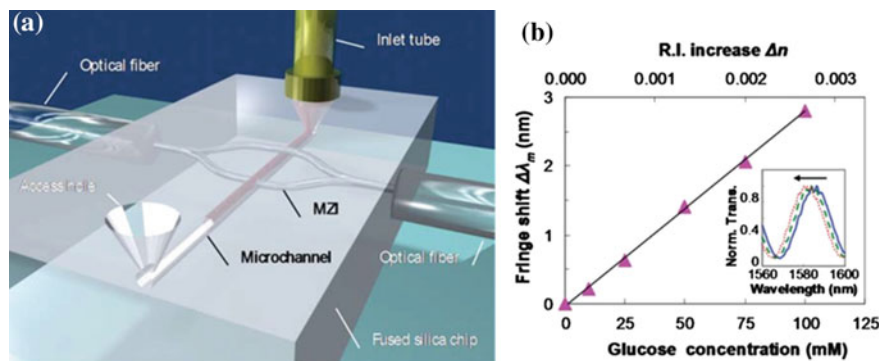


Fig. 6.12 **a** Schematic of the microfluidic channel integrated with a Mach-Zehnder interferometer for refractive index measurements. Figure **b** displays the fringe shift as a function of glucose-D concentration for the device shown in **(a)**. Reproduced from [16] with permission of ©The Royal Society of Chemistry

etching effect to produce microresonators in fused silica. These were fabricated by laser-writing the negative image of the final structure and by etching it, leaving a microdisk supported by thin pillars on top of the silica surface. The structures were then annealed with the aid of a CO_2 laser to improve the cavities surface smoothness. However, during this process, surface tension induced a collapse of the disk leading to a toroid-shaped boundary (Fig. 6.13a). Using the optical fiber taper coupling method, they generated whispering gallery modes in the 1530–1565 nm range with a quality factor of 1.07×10^6 . One of the limitations is the long time necessary to fabricate the microresonators (6 h in this case). Therefore, two-photon polymerization, assisted by fs-laser writing, has been proposed for the production of these structures. Liu et al. [93] fabricated microcavities in sol-gel deposited on a zirconium/silicon substrate and obtained a quality factor of 1.48×10^5 in the 1550 nm band range. Grossmann et al. [94] also fabricated a microcavity in Ormocomp, a negative-tone photoresist, deposited on a silicon wafer with a quality factor of 1.2×10^6 in the 1300 nm wavelength region.

Song et al. [95] used these microresonators to produce an optofluidic sensor in a fused silica chip. A Y-branched channel, with two inlets for fluid injection, was fabricated using the FLICE technique. The channel outlet port was fabricated closely to a reservoir, where the microresonator was produced in order for light to interact with the fluid; the microresonator was also fabricated using the FLICE technique. A design of the proposed sensor is shown in Fig. 6.13b. To excite whispering gallery modes, a fiber taper was brought to the vicinity of the microresonator, and both were welded by CO_2 laser irradiation. In the final structure, a quality factor of 3.21×10^5 was measured in air. In order to demonstrate refractive index sensing, the channel was filled with purified water mixed with salt. Variations of the salt concentration induced a shift on the wavelength of the mode coupled to the microresonator from

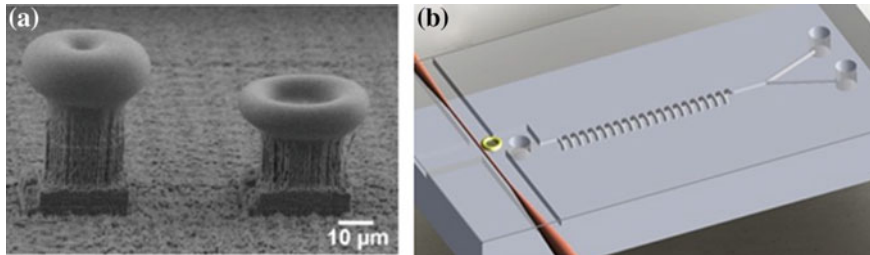


Fig. 6.13 **a** SEM image of two microresonators made in fused silica after CO₂ laser annealing. **b** Schematic of the integrated optofluidic sensor proposed by Song et al. [95]. Images (a) and (b) were reproduced from [92, 95], respectively, with permission from The Optical Society (© 2012 Optical Society of America, © 2014 Optical Society of America)

the fiber, and a linear sensitivity of 220 nm/RIU was obtained, yielding a detection limit of 1.2×10^{-4} RIU.

The high quality factor provided by these structures makes them also attractive for the production of active whispering gallery mode microcavities, with lasing sources having already been produced in dye-doped resins with emission at 639 nm and in doped Nd:YAG glass with emission at 1550 nm [96, 97].

SERS (Surface-enhanced Raman Spectroscopy) micromonitors for detection of biomolecules have also been demonstrated by Xu et al. [98]. Production of this device involved the following steps: (i) a microfluidic channel in a glass substrate was produced by photolithography and etching, (ii) then a silver nitrate solution was injected in the channel, (ii) fs-laser writing induced photoreduction of the irradiated silver particles that deposited in the channel surface (Fig. 6.14a). The device was used to detect p-aminothiophenol (p-ATP) and flavin adenine dinucleotide (FAD) molecules, in two separate experiments. The molecules were injected in the channel and adsorbed to the metal surface. An ion laser, emitting at 514 nm, was then focused inside the channel through an objective lens, which was also used to collect scattering light (Fig. 6.14b). Both molecules were detected with an enhancement factor around 10^8 and a detection limit around the nanomolar range. The high surface roughness of the silver layer was shown to enhance the detection limit.

Recently, fs-laser micromachining has also been applied for the formation of 3D photonic crystals. This structure consists of a three-dimensional periodic modulation of the refractive index, and is characterized by a photonic band gap that inhibits light propagation at a certain wavelength. This wavelength depends on the index contrast between the two materials that compose the photonic crystal, which makes these structures attractive for sensing applications. Haque et al. [99] fabricated a woodpile structure in SU-8 photoresist by two-photon polymerization. The photonic crystal was produced inside a microfluidic channel and was interrogated by an optical waveguide (Fig. 6.15a). Both structures were made in a fused silica chip by fs-laser micromachining. Light propagating through the waveguide could transverse the photonic crystal, where the existence of the photonic band gap led to dips in

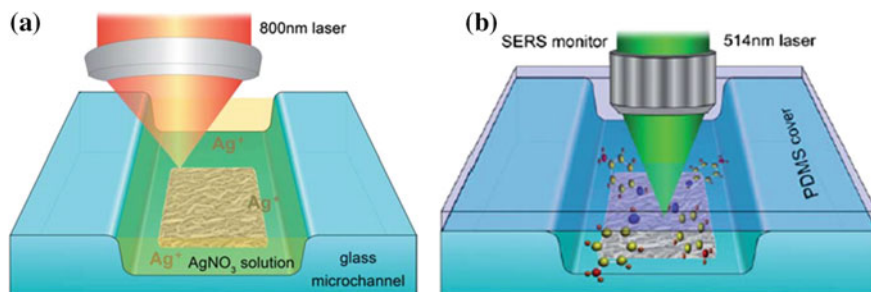


Fig. 6.14 Schematics of **a** silver layer patterning by fs-laser writing and of **b** target molecule detection through SERS. Reproduced from [98] with permission of ©The Royal Society of Chemistry

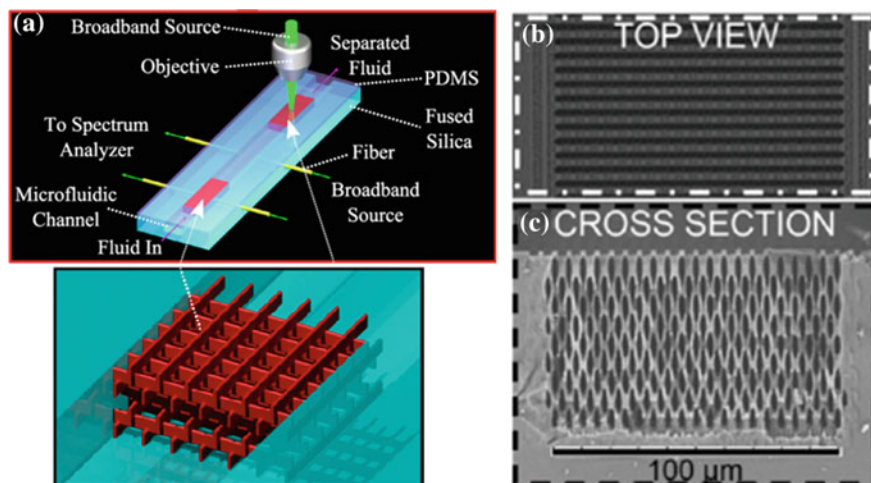


Fig. 6.15 Schematic of the integrated optofluidic device proposed by Haque et al. [99], with a zoom-in image of the proposed woodpile structure. SEM **b** top view image and **c** cross-section image of the inverted woodpile structure fabricated in fused silica by Ho et al. [100]. Images (a) and (b) were reproduced from [99, 100], respectively, with permission from The Optical Society (© 2013 OSA, © 2012 Optical Society of America)

the transmission spectrum. Theoretical results show that a sensitivity as high as 725 nm/RIU can be obtained. Some limitations of this technique are the low index contrast provided by the SU-8 photoresist, which contributes to a weaker band gap, and shrinkage of the polymer, which disturbs the lattice periodicity. Ho et al. [100] also fabricated an inverted-woodpile structure embedded in a microfluidic channel made in a fused silica chip (Fig. 6.15b). The photonic crystal structure was made based on the etching selectivity modification induced by fs-laser writing. The crystal was written layer-by-layer, which revealed that the processing conditions (scanning speed and pulse energy) had to be changed in order to maintain the hole width and height constant.

6.4 Conclusions

As shown in this chapter, fs-laser micromachining is a powerful microfabrication technique with a broad range of applications, which extend from optics and photonics to biology and analytical chemistry. The use of ultrashort pulse widths and extremely high peak intensities, gives rise to a non-linear interaction that can generate several kinds of modifications in the material structure. This laser-induced modification occurs within a submicrometer resolution, and can enable formation of (i) passive or active optical circuits due to a smooth variation of the refractive index, or of (ii) microfluidic systems combined with polymeric structures to mix or filter particles or to control the flow rate, due to the generation of etching selectivity and to a laser-induced localized polymerization reaction.

The possibility to fabricate three-dimensional components and integrate them in a single glass block has also extended the applications of this technique to the field of lab-on-a-chip devices. As demonstrated, several optofluidic devices for cell manipulation and behaviour analysis or for label-free detection have already been reported, which show the potential of this technique in the biomedical field [101]. Nevertheless, improvements on these devices can still be made. For instance, integration of microfluidics with biochemistry skills for formation of organ-on-a-chip devices is highly regarded for the study of biological micro- and nano-environments [102, 103].

Acknowledgements Project “NanoSTIMA: Macro-to-Nano Human Sensing Towards Integrated Multimodal Health Monitoring and Analytics/NORTE-01-0145-FEDER-000016” is financed by the North Portugal Regional Operational Programme (NORTE 2020), under the PORTUGAL 2020 Partnership Agreement, and through the European Regional Development Fund (ERDF). João M. Maia acknowledges the support of the Foundation for Science and Technology (FCT), Portugal through the Investigation Grant PD/B1/128995/2017.

References

1. G.M. Whitesides, *Nature* **442**(7101), 368–373 (2006)
2. P.S. Dittrich, A. Manz, *Nat. Rev. Drug Discov.* **5**(3), 210–218 (2006)
3. T.M. Squires, S.R. Quake, *Rev. Mod. Phys.* **77**(3), 977–1026 (2005)
4. P. Yager, T. Edwards, E. Fu, K. Helton, K. Nelson, M.R. Tam, B.H. Weigl, *Nature* **442**(7101), 412–418 (2006)
5. J. Wu, M. Gu, *J. Biomed. Opt.* **16**(8), (2011)
6. K. De Vos, I. Bartolozzi, E. Schacht, P. Bienstman, R. Baets, *Opt. Express* **15**(12), 7610–7615 (2007)
7. S. Suzuki, A. Sugita, *NTT Tech. Rev.* **3**(7), 12–16 (2005)
8. D.C. Duffy, J.C. McDonald, O.J.A. Schueller, G.M. Whitesides, *Anal. Chem.* **70**(23), 4974–4984 (1998)
9. H. Becker, L.E. Locascio, *Talanta* **56**(2), 267–287 (2002)
10. D. Tan, K.N. Sharafudeen, Y. Yue, J. Qiu, *Prog. Mater. Sci.* **75**, 154–228 (2016)

11. K.M. Davis, K. Miura, N. Sugimoto, K. Hirao, *Opt. Lett.* **21**(21), 1729–1731 (1996)
12. J. Xu, D. Wu, Y. Hanada, C. Chen, S. Wu, Y. Cheng, K. Sugioka, K. Midorikawa, *Lab Chip* **13**(23), 4608–4616 (2013)
13. A. Marcinkevičius, S. Juodkakis, M. Watanabe, M. Miwa, S. Matsuo, H. Misawa, J. Nishii, *Opt. Lett.* **26**(5), 277–279 (2001)
14. K. Sugioka, J. Xu, D. Wu, Y. Hanada, Z. Wang, Y. Cheng, K. Midorikawa, *Lab Chip* **14**(18), 3447–3458 (2014)
15. N. Bellini, K.C. Vishnubhatla, F. Bragheri, L. Ferrara, P. Minzioni, R. Ramponi, I. Cristiani, R. Osellame, *Opt. Express* **18**(5), 4679–4688 (2010). <https://doi.org/10.1364/OE.18.004679>
16. A. Crespi, Y. Gu, B. Ngamsom, H.J.W.M. Hoekstra, C. Dongre, M. Pollnau, R. Ramponi, H.H. Van Den Vlekkert, P. Watts, G. Cerullo, R. Osellame, *Lab Chip* **10**(9), 1167–1173 (2010). <https://doi.org/10.1039/B920062B>
17. S. Ho, P.R. Herman, J.S. Aitchison, *Appl. Phys. A* **106**(1), 5–13 (2012)
18. K. Itoh, W. Watanabe, S. Nolte, C.B. Schaffer, *MRS Bull.* **31**(8), 620–625 (2006)
19. J.W. Chan, T. Huser, S. Risbud, D.M. Krol, *Opt. Lett.* **26**(21), 1726–1728 (2001)
20. A. Agarwal, M. Tomozawa, *J. Non-Cryst. Solids* **209**(1–2), 166–174 (1997)
21. K. Hirao, K. Miura, *J. Non-Cryst. Solids* **239**(1–3), 91–95 (1998)
22. T. Fukuda, S. Ishikawa, T. Fujii, K. Sakuma, H. Hosoya, Photon processing in microelectronics and photonics III, in *Proceedings of SPIE*, vol. 5339, 15 July 2004
23. Y. Nasu, M. Kohtoku, Y. Hibino, *Opt. Lett.* **30**(7), 723–725 (2005)
24. R.R. Thomson, H.T. Bookey, N.D. Psaila, A. Fender, S. Campbell, W.N. MacPherson, J.S. Barton, D.T. Reid, A.K. Kar, *Opt. Express* **15**(18), 11691–11697 (2007)
25. S.M. Eaton, H. Zhang, P.R. Herman, *Opt. Express* **13**, 4708–4716 (2005)
26. M. Ams, G.D. Marshall, D.J. Spence, M.J. Withford, *Opt. Express* **13**(15), 5676–5681 (2005)
27. S.M. Eaton, M.L. Ng, R. Osellame, P.R. Herman, *J. Non-Cryst. Solids* **357**(11–13), 2387–2391 (2011)
28. M. Ams, P. Dekker, S. Gross, M.J. Withford, *Nanophotonics* (to be published) (2017)
29. J.R. Grenier, L.A. Fernandes, J.S. Aitchison, P.V.S. Marques, P.R. Herman, *Opt. Lett.* **37**(12), 2289–2291 (2012)
30. P. Zeil, C. Voigtländer, J. Thomas, D. Richter, S. Nolte, *Opt. Lett.* **38**(13), 2354–2356 (2013)
31. L.A. Fernandes, J.R. Grenier, P.R. Herman, J.S. Aitchison, P.V.S. Marques, *Opt. Express* **19**(19), 18294–18301 (2011)
32. I.-B. Sohn, M.-S. Lee, J. Chung, *IEEE Photon. Technol. Lett.* **17**(11), 2349–2351 (2005)
33. J. Liu, Z. Zhang, S. Chang, C. Fluerau, C.P. Grover, *Opt. Commun.* **253**(4–6), 315–319 (2005)
34. V.A. Amorim, J.M. Maia, D. Alexandre, P.V.S. Marques, *I.E.E.E. Photon. Technol. Lett.* **29**(7), 619–622 (2017)
35. K. Suzuki, V. Sharma, J.G. Fujimoto, E.P. Ippen, Y. Nasu, *Opt. Express* **14**(6), 2335–2343 (2006)
36. W.-J. Chen, S.M. Eaton, H. Zhang, P.R. Herman, *Opt. Express* **16**(15), 11470–11480 (2008)
37. W. Watanabe, Y. Note, K. Itoh, *Opt. Lett.* **30**(21), 2888–2890 (2005)
38. D.-Y. Liu, Y. Li, Y.-P. Dou, H.-C. Guo, H. Yang, Q.-H. Gong, *Chin. Phys. Lett.* **25**(7), 2500–2503 (2008)
39. V.A. Amorim, J.M. Maia, D. Alexandre, P.V.S. Marques, *J. Lightwave Technol.* **35**(17), 3615–3621 (2017)
40. G. Douglass, F. Dreisow, S. Gross, S. Nolte, M.J. Withford, Rapid prototyping of arrayed waveguide gratings, *Paper presented at Photonic and Fiber Technology 2016*, Sydney, Australia, 5–8 Sept 2016
41. S.-L. Li, P. Han, M. Shi, Y. Yao, B. Hu, M. Wang, X. Zhu, *Opt. Express* **19**(24), 23958–23964 (2011)
42. J. Burghoff, S. Nolte, A. Tünnermann, *Appl. Phys. A* **89**(1), 127–132 (2007). <https://doi.org/10.1007/s00339-007-4152-0>
43. A.G. Okhrimchuk, A.V. Shestakov, I. Khrushchev, J. Mitchell, *Opt. Lett.* **30**(17), 2248–2250 (2005)

44. M.-M. Dong, C.-W. Wang, Z.-X. Wu, Y. Zhang, H.-H. Pan, Q.-Z. Zhao, *Opt. Express* **21**(13), 15522–15529 (2013)
45. R. Osellame, G. Della Valle, N. Chiodo, S. Taccheo, P. Laporta, O. Svelto, G. Cerullo, *Appl. Phys. A* **93**(1), 17–26 (2008)
46. D. Choudhury, J.R. Macdonald, A.K. Kar, *Laser Photon. Rev.* **8**(6), 827–846 (2014)
47. C. Zhang, N. Dong, J. Yang, F. Chen, J.R.V. De Aldana, Q. Lu, *Opt. Express* **19**(13), 12503–12508 (2011)
48. G. Palmer, S. Gross, A. Fuerbach, D.G. Lancaster, M.J. Withford, *Opt. Express* **21**(14), 17413–17420 (2013)
49. G. Della Valle, S. Taccheo, R. Osellame, A. Festa, G. Cerullo, P. Laporta, *Opt. Express* **15**(6), 3190–3194 (2007)
50. B. McMillen, B. Zhang, K.P. Chen, A. Benayas, D. Jaque, *Opt. Lett.* **37**(9), 1418–1420 (2012)
51. M.A. Hughes, W. Yang, D.W. Hewak, *J. Opt. Soc. Am. B* **26**(7), 1370–1378 (2009)
52. N.D. Psaila, R.R. Thomson, H.T. Bookey, S. Shen, N. Chiodo, R. Osellame, G. Cerullo, A. Jha, A.K. Kar, *Opt. Express* **15**(24), 15776–15781 (2007)
53. H.T. Bookey, R.R. Thomson, N.D. Psaila, A.K. Kar, N. Chiodo, R. Osellame, G. Cerullo, *I.E.E.E. Photon. Technol. Lett.* **19**(12), 892–894 (2007)
54. W. Horn, S. Kroesen, J. Herrmann, J. Imbrock, C. Denz, *Opt. Express* **20**(24), 26922–26928 (2012)
55. R. Taylor, C. Hnatovsky, E. Simova, *Laser Photon. Rev.* **2**(1–2), 26–46 (2008)
56. A.A. Said, M. Dugan, P. Bado, Y. Bellouard, A. Scott, J.R. Mabesa Jr., *Photon processing in microelectronics and photonics III*, in *Proceedings of SPIE*, vol. 5339, 15 July 2004
57. B. Fissette, M. Meunier, *Photonics north 2004: photonic applications in astronomy, biomedicine, imaging, materials processing, and education*, in *Proceedings of SPIE*, vol. 5578, 9 Dec 2004
58. K. Sugioka, Y. Cheng, K. Midorikawa, *Appl. Phys. A* **81**(1), 1–10 (2005)
59. S. Matsuo, Y. Tabuchi, T. Okada, S. Juodkazis, H. Misawa, *Appl. Phys. A* **84**(1–2), 99–102 (2006)
60. D. Wortmann, J. Gottmann, N. Brandt, H. Horn-Solle, *Opt. Express* **16**(3), 1517–1522 (2008)
61. D. Choudhury, A. Rodenas, L. Paterson, F. Díaz, D. Jaque, A.K. Kar, *Appl. Phys. Lett.* **103**(4) (2013)
62. Y. Bellouard, A. Said, M. Dugan, P. Bado, *Opt. Express* **12**(10), 2120–2129 (2004)
63. Y. Bellouard, A.A. Said, M. Dugan, P. Bado, *Commercial and biomedical applications of ultrafast lasers VI*, in *Proceedings of SPIE*, vol. 6108, 28 Feb 2006
64. C. Hnatovsky, R.S. Taylor, E. Simova, V.R. Bhardwaj, D.M. Rayner, P.B. Corkum, *Opt. Lett.* **30**(14), 1867–1869 (2005)
65. J.M. Maia, V.A. Amorim, D. Alexandre, P.V.S. Marques, in *Proceedings of the 5th International Conference on Photonics, Optics and Laser Technology (PHOTOPTICS 2017)*, 27 Feb–1 Mar 2017
66. A. Champion, M. Beresna, P. Kazansky, Y. Bellouard, *Opt. Express* **21**(21), 24942–24951 (2013)
67. F. He, J. Lin, Y. Cheng, *Appl. Phys. B* **105**(2), 379–384 (2011)
68. K.C. Vishnubhatla, N. Bellini, R. Ramponi, G. Cerullo, R. Osellame, *Opt. Express* **17**(10), 8685–8695 (2009)
69. S. Kiyama, S. Matsuo, S. Hashimoto, Y. Morihira, *J. Phys. Chem. C* **113**(27), 11560–11566 (2009)
70. Y. Temiz, R.D. Lovchik, G.V. Kaigala, E. Delamarche, *Microelectron. Eng.* **132**, 156–175 (2015)
71. M. Masuda, K. Sugioka, Y. Cheng, N. Aoki, M. Kawachi, K. Shihoyama, K. Toyoda, H. Helvajian, K. Midorikawa, *Appl. Phys. A* **76**(5), 857–860 (2003)
72. K. Liu, Q. Yang, S. He, F. Chen, Y. Zhao, X. Fan, L. Li, C. Shan, H. Bian, *Microsyst. Technol.* **19**(7), 1033–1040 (2013)
73. Y. Li, K. Itoh, W. Watanabe, K. Yamada, D. Kuroda, J. Nishii, Y. Jiang, *Opt. Lett.* **26**(23), 1912–1914 (2001)

74. Y. Li, S. Qu, *Curr. Appl. Phys.* **13**(7), 1292–1295 (2013)
75. K.-S. Lee, R.H. Kim, D.-Y. Yang, S.H. Park, *Prog. Polym. Sci.* **33**(6), 631–681 (2008)
76. J. Wang, Y. He, H. Xia, L.-G. Niu, R. Zhang, Q.-D. Chen, Y. Zhang, Y.-F. Li, S.-J. Zeng, J.-H. Qin, B.-C. Lin, H.-B. Sun, *Lab Chip* **10**(15), 1993–1996 (2010). <https://doi.org/10.1039/C003264F>
77. L. Amato, Y. Gu, N. Bellini, S.M. Eaton, G. Cerullo, R. Osellame, *Lab Chip* **12**(6), 1135–1142 (2012)
78. T.W. Lim, Y. Son, Y.J. Jeong, D.-Y. Yang, H.-J. Kong, K.-S. Lee, D.-P. Kim, *Lab Chip* **11**(1), 100–103 (2011). <https://doi.org/10.1039/C005325M>
79. D. Wu, S.-Z. Wu, J. Xu, L.-G. Niu, K. Midorikawa, K. Sugioka, *Laser Photon. Rev.* **8**(3), 458–467 (2014)
80. R.W. Applegate Jr., J. Squier, T. Vestad, J. Oakey, D.W.M. Marr, P. Bado, M.A. Dugan, A.A. Said, *Lab Chip* **6**(3), 422–426 (2006). <https://doi.org/10.1039/B512576F>
81. D.J. Hwang, M. Kim, K. Hiromatsu, H. Jeon, C.P. Grigoropoulos, *Appl. Phys. A* **96**(2), 385–390 (2009). <https://doi.org/10.1007/s00339-009-5210-6>
82. M. Kim, D.J. Hwang, H. Jeon, K. Hiromatsu, C.P. Grigoropoulos, *Lab Chip* **9**(2), 311–318 (2009). <https://doi.org/10.1039/B808366E>
83. F. Bragheri, L. Ferrara, N. Bellini, K.C. Vishnubhatla, P. Minzioni, R. Ramponi, R. Osellame, I. Cristiani, *J. Biophotonics* **3**(4), 234–243 (2010)
84. F. Bragheri, P. Minzioni, R. Martinez Vazquez, N. Bellini, P. Paiè, C. Mondello, R. Ramponi, I. Cristiani, R. Osellame, *Lab Chip* **12**(19), 3779–3784 (2012). <https://doi.org/10.1039/c2lc40705a>
85. T. Yang, P. Paiè, G. Nava, F. Bragheri, R.M. Vazquez, P. Minzioni, M. Vegliione, M. Di Tano, C. Mondello, R. Osellame, I. Cristiani, *Lab Chip* **15**(5), 1262–1266 (2015)
86. R.M. Vazquez, R. Osellame, D. Nolli, C. Dongre, H. Van Den Vlekkert, R. Ramponi, M. Pollnau, G. Cerullo, *Lab Chip* **9**(1), 91–96 (2009)
87. C. Dongre, R. Dekker, H.J.W.M. Hoekstra, M. Pollnau, R. Martinez-Vazquez, R. Osellame, G. Cerullo, R. Ramponi, R. Van Weeghel, G.A.J. Besselink, H.H. Van Den Vlekkert, *Opt. Lett.* **33**(21), 2503–2505 (2008). <https://doi.org/10.1364/OL.33.002503>
88. C. Dongre, J. Van Weerd, G.A.J. Besselink, R. Van Weeghel, R.M. Vazquez, R. Osellame, G. Cerullo, M. Cretich, M. Chiari, H.J.W.M. Hoekstra, M. Pollnau, *Electrophoresis* **31**(15), 2584–2588 (2010)
89. V. Maselli, J.R. Grenier, S. Ho, P.R. Herman, *Opt. Express* **17**(14), 11719–11729 (2009)
90. J.M. Maia, V.A. Amorim, D. Alexandre, P.V.S. Marques, *J. Lightwave Technol.* **35**(11), 2291–2298 (2017)
91. Y. Hanada, K. Sugioka, K. Midorikawa, *Lab Chip* **12**(19), 3688–3693 (2012). <https://doi.org/10.1039/C2LC40377C>
92. J. Lin, S. Yu, Y. Ma, W. Fang, F. He, L. Qiao, L. Tong, Y. Cheng, Z. Xu, *Opt. Express* **20**(9), 10212–10217 (2012). <https://doi.org/10.1364/OE.20.010212>
93. Z.-P. Liu, Y. Li, Y.-F. Xiao, B.-B. Li, X.-F. Jiang, Y. Qin, X.-B. Feng, H. Yang, Q. Gong, *Appl. Phys. Lett.* **97**(21) (2010)
94. T. Grossmann, S. Schleede, M. Hauser, T. Beck, M. Thiel, G. Von Freymann, T. Mappes, H. Kalt, *Opt. Express* **19**(12), 11451–11456 (2011)
95. J. Song, J. Lin, J. Tang, Y. Liao, F. He, Z. Wang, L. Qiao, K. Sugioka, Y. Cheng, *Opt. Express* **22**(12), 14792–14802 (2014). <https://doi.org/10.1364/OE.22.014792>
96. J.-F. Ku, Q.-D. Chen, R. Zhang, H.-B. Sun, *Opt. Lett.* **36**(15), 2871–2873 (2011)
97. J. Lin, Y. Xu, J. Song, B. Zeng, F. He, H. Xu, K. Sugioka, W. Fang, Y. Cheng, *Opt. Lett.* **38**(9), 1458–1460 (2013)
98. B.-B. Xu, Z.-C. Ma, L. Wang, R. Zhang, L.-G. Niu, Z. Yang, Y.-L. Zhang, W.-H. Zheng, B. Zhao, Y. Xu, Q.-D. Chen, H. Xia, H.-B. Sun, *Lab Chip* **11**(19), 3347–3351 (2011). <https://doi.org/10.1039/C1LC20397E>
99. M. Haque, N.S. Zacharia, S. Ho, P.R. Herman, *Biomed. Opt. Express* **4**(8), 1472–1485 (2013). <https://doi.org/10.1364/BOE.4.001472>

100. S. Ho, M. Haque, P.R. Herman, J.S. Aitchison, *Opt. Lett.* **37**(10), 1682–1684 (2012). <https://doi.org/10.1364/OL.37.001682>
101. F. Sima, J. Xu, D. Wu, K. Sugioka, *Micromachines* **8**(2), (2017)
102. D. Huh, G.A. Hamilton, D.E. Ingber, *Trends Cell Biol.* **21**(12), 745–754 (2011)
103. D.J. Beebe, D.E. Ingber, J. Den Toonder, *Lab Chip* **13**(18), 3447–3448 (2013)